NANO · MICRO small
www.small-journal.com

Molecular Programming of Biodegradable Nanoworms via Ionically Induced Morphology Switch toward Asymmetric Therapeutic Carriers

Shoupeng Cao, Jingxin Shao, Yifeng Xia, Hailong Che, Zhiyuan Zhong, Fenghua Meng, Jan C. M. van Hest, Loai K. E. A. Abdelmohsen,* and David S. Williams**

Engineering biodegradable nanostructures with precise morphological characteristics is a key objective in nanomedicine. In particular, asymmetric (i.e., nonspherical) nanoparticles are desirable due to the advantageous effects of shape in a biomedical context. Using molecular engineering, it is possible to program unique morphological features into the self-assembly of block copolymers (BCPs). However, the criteria of biocompatibility and scalability limit progress due to the prevalence of nondegradable components and the use of toxic solvents during fabrication. To address this shortfall, a robust strategy for the fabrication of morphologically asymmetric nanoworms, comprising biodegradable BCPs, has been developed. Modular BCPs comprising poly (ethylene glycol)-block-poly(caprolactone-gradient-trimethylene carbonate) (PEG–PCLgTMC), with a terminal chain of quaternary ammonium-TMC (PTMC-Q), undergo self-assembly via direct hydration into well-defined nanostructures. By controlling the solution ionic strength during hydration, particle morphology switches from spherical micelles to nanoworms (of varying aspect ratio). This ionically-induced switch is driven by modulation of chain packing with salts screening interchain repulsions, leading to micelle elongation. Nanoworms can be loaded with cytotoxic cargo (e.g., doxorubicin) at high efficiency, preferentially interact with cancer cells, and increase tumor penetration. This work showcases the ability to program assembly of BCPs and the potential of asymmetric nanosystems in anticancer drug delivery.

1. Introduction

Precisely controlling the morphology of self-assembled polymer architectures is becoming a key paradigm for the design of nanomedical therapies, due to the important role parameters such as size, shape, surface chemistry, and ligand density have on performance in vivo.[1] Significant advances have been made using asymmetric particles as the basis for therapeutic nanosystems due to their ability to successfully navigate key biological barriers and enhance the efficacy of specific interactions with target tissues.[2] For instance, high aspect ratio nanostructures have been shown to result in enhanced specific accumulation and reduced nonspecific adhesion to cells, while displaying distinct uptake mechanisms.[3] The potential for asymmetric nanoparticles to improved therapeutic outcomes in, for example, anticancer drug delivery fuels interest in the development of new processes for their manufacture.[4] Different processes have been developed for the manufacture asymmetric microparticles, such as PRINT.[5] Another versatile approach involves block copolymers that undergo directed self-assembly (based upon physicochemical parameters associated with chain packing and intermolecular interactions); this facilitates bottom-up programming of asymmetric nanosystems with versatile functionality.[6] Specific examples include polymerization induced self-assembly,[7] crystallization-driven self-assembly,[8] or osmotically induced shape transformation processes,[9] which result in asymmetric

S. Cao, Dr. J. Shao, H. Che, Prof. J. C. M. van Hest, Dr. L. K. E. A. Abdelmohsen
Bio-Organic Chemistry
Institute for Complex Molecular Systems
Institution, Eindhoven University of Technology
P.O. Box 513 (STO 3.41), 5600 MB Eindhoven, the Netherlands
E-mail: j.c.m.v.hest@tue.nl; l.k.e.a.abdelmohsen@tue.nl

The ORCID identification number(s) for the author(s) of this article can be found under https://doi.org/10.1002/smll.201901849.

DOI: 10.1002/smll.201901849

Y. Xia, Prof. Z. Zhong, Prof. F. Meng
Biomedical Polymers Laboratory
and Jiangsu Key Laboratory of Advanced Functional Polymer
Design and Application
College of Chemistry
Chemical Engineering and Materials Science
Soochow University
Suzhou 215123, P. R. China

Dr. D. S. Williams
Department of Chemistry
College of Science
Swansea University
Swansea SA2 8PP, UK
E-mail: d.s.williams@swansea.ac.uk

particles.[10] At present, there is however a dearth of polymeric technologies that have reached the market due to problems associated with producibility, toxicity, and/or reproducibility—arising from the tendency for copolymer engineering to focus on the use of nonbiodegradable components and fabrication processes that introduce toxic solvents and result in nonuniform products.

In order to overcome these barriers, we have recently developed technology for the formation of biodegradable nanovectors that can be fabricated using the direct hydration (DH) methodology.[11] The DH methodology circumvents the use of toxic organic solvents and is a major step toward achieving controlled self-assembly under more biocompatible conditions. Block copolymers (BCPs) comprising poly(ethylene glycol)-poly(trimethylene carbonate) (PEG-PTMC) were utilized as the structural basis for drug-loaded nanovectors (NVs) that were fabricated using DH, whereby dissolution in oligo(ethylene glycol) (OEG) preceded addition of buffer and formation of pristine particles that did not require any further purification prior to use in vitro or in vivo. Due to the highly uniform nature of PEG-PTMC copolymers that were prepared it was possible to precisely control the size of the resulting NVs; however, additional strategies are required to incorporate advanced characteristics, such as shape, into this system.[12] Precision engineering of BCPs into well-defined (nano)morphologies is relatively unexplored—especially when using strictly biodegradable components and using the DH approach for particle fabrication.

In terms of BCP programming, self-assembly of amphiphilic copolymers is driven by hydrophobic self-association and modulated by the steric forces associated with the hydrated surface blocks. Systematic introduction of chemical triggers (such as pH-responsive, thermally responsive, or ionic subunits) can be used to direct BCP assembly, engineering "smart" nanostructures that are sensitive to their environment.[13] In particular, directing the self-assembly of BCPs by modulating their amphiphilic nature, tailoring interactions with ions in solution, is an effective strategy to control particle morphology.[3b,14] Tailoring the concentration and nature of aqueous ions is a simple and effective strategy to achieve controlled self-assembly and dictate the final morphology of BCP assemblies.[3c] In recent work, we have demonstrated that osmotically induced shape transformation can be applied to spherical polymersomes in order to direct formation of either nanotubes or bowl-shaped stomatocytes, driven by the influence of salts and solvent composition on BCP packing.[9a,15]

Inspired by this, we here report a strategy for the controlled formation of biodegradable nanoworms using an ionically induced trigger directing the packing of a tertiary chain comprising cationic derivatives of PTMC (PTMC-Q) (Figure 1). Molecular programming of BCPs provides a novel route toward the formation of cationic, asymmetric nanoworms, an exciting platform for applications in nanomedicine where the elongated nanostructures and positive charge can enhance interactions with cellular surfaces and drive integration of therapeutic cargo.[16] Furthermore, due to the increasingly negative charge of cancer cell membranes, nanoparticles bearing controlled degrees of positive charge are capable of electrostatically driven specificity, a morphology driven (as opposed to ligand affinity) targeting mechanism.[17]

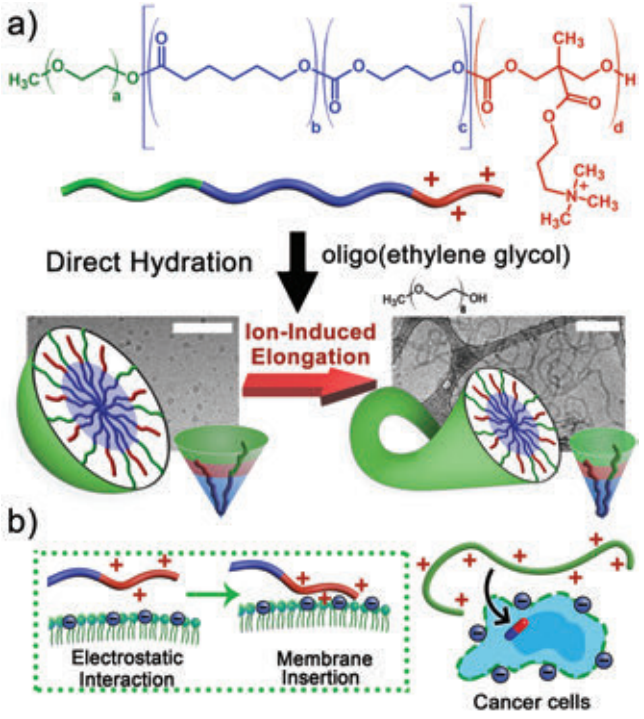

Figure 1. Programming the formation of biodegradable nanoworms via an ionically induced morphology switch toward asymmetric therapeutic carriers. a) Terpolymer chemical structure and ionically induced morphology switch between spherical micelles and nanoworms due to modulation of interchain interactions (due to the presence of quaternary ammonium block) in the absence/presence of NaCl. b) The proposed membrane interactions between cationic nanoworms and (negatively charged) cancer cell membranes leading to enhanced membrane permeability and preferential delivery of therapeutic payloads. (Scale bars = 200 nm)

2. Results and Discussion

2.1. Molecular Programming of BCPs

Molecular programming of BCPs was accomplished using a modular polymerization approach; producing amphiphilic terpolymers with well-defined chemical characteristics (cf. Supporting Information). Poly(ethylene glycol)-block-poly(caprolactone-gradient-trimethylene carbonate) (PEG-PCL*g*TMC) copolymers were utilized as the basis for this system due to their established capacity in generating well-defined polymer assemblies (using the DH process) and their biodegradability/biocompatibility.[11,18] Although PCL is a crystalline polymer, PTMC counteracts this property by providing the necessary fluidity to enable effective chain packing whilst maintaining the rigidity necessary to generate higher order polymeric nanostructures like polymersomes.[11,19] Conversely, copolymers comprising PEG–PTMC alone will only form spherical micelles due to the flexibility of the PTMC block.[12a] As we have demonstrated, copolymers of PCL and PTMC can (under certain conditions) form worm-like structures; however, isolating the worm phase is challenging and requires an additional strategy to balance bilayer rigidity with the high surface curvature required for micelle formation.[11] To accomplish

this, we utilized copolymers based upon PEG_{22}-$PCL_{30}gTMC_{30}$ (≈7.5 kDa, termed as $TerP_{22}$) for the engineering of asymmetric nanoparticles. $PCL_{30}gTMC_{30}$ provide sufficient flexibility to maintain the hydrophobic bilayer over extended length scales. Using $TerP_{22}$ as a macroinitiator a bromide functional TMC derivative was polymerized onto the PTMC chain end.[20] Via a nucleophilic substitution reaction, the bromides were replaced by quaternary ammonium groups in order to provide the enhanced surface curvature required to generate (high surface curvature) micellar architectures. A series of well-defined (Đ ≈ 1.1) terpolymers ($TerP_{22}$-Q) was prepared in which the length of the ternary block was systematically varied yielding $TerP_{22}$-Q_n BCPs (where n = 6, 11, and 20 repeats), to investigate the effect of hydrophilic portion and charge density on the self-assembly process (Scheme S1, Supporting Information).[16a] Because electrostatic repulsions between the highly charged PTMC-Q blocks will induce the formation of high surface curvature nanoparticles (i.e., micelles), we anticipate that the concentration of salt present during formation (screening electrostatic repulsions) will be a key factor in controlling assembly of these $TerP_{22}$-Q copolymers.

2.2. Nanoworms Formation via Direct Hydration

$TerP_{22}$-Q BCPs were all compatible with the DH process, whereby a 10 wt% solution was prepared in oligo (ethylene glycol) (OEG) prior to addition of water (or salt solution) and stirring at room temperature for 5 min. $TerP_{22}$-Q BCPs were hydrated using solutions of increasing [NaCl] from 0–400 × 10^{-3} M in order to determine the effect of ionic strength on self-assembly. From dynamic light scattering (DLS) data it was evident that the structural evolution using all three copolymers was significantly different. In general terms, under conditions where the molecular volume of a hydrophilic copolymer block increases (e.g., due to increased molecular weight or hydration) dynamic assembly tends to favor the (high surface curvature) spherical micelle phase, where the packing parameter (P) ≤ 1/3. Under conditions where the hydrophilic volume decreases (or hydrophobic volume increases), lower surface curvature phases like elongated worms (or vesicles) are favored.[21] First, terpolymers bearing the longest PTMC-Q terminal block ($TerP_{22}$-Q_{20}) appeared to form uniform micelles under all conditions with nearly the same hydrodynamic radius of ≈25–30 nm (Figure S17a–c). $TerP_{22}$-Q_{20} did not undergo transformation into asymmetric particles due to the strong repulsions between cationic chains and the large hydrophilic volume, maximizing surface curvature (i.e., spherical micelles, SMs). Cryo-TEM microscopy confirmed the presence of SMs in samples of $TerP_{22}$-Q_{20} (Figure S17d, Supporting Information), and quantitative insight was obtained using asymmetric flow field-flow fractionation (AF4) coupled with multiangle light scattering (MALS) and DLS. Measurements of the shape factor (ρ) provided insight into nanoparticle shape by comparison of the radius of gyration (R_g) and R_h ($\rho = R_g/R_h$). Indeed, $TerP_{22}$-Q_{20} SMs (hydrated into water or 200 × 10^{-3} M NaCl) eluted after 10–12 min with ρ values ranging from 0.7 to 0.75, indicative of micelles that possess a dense core and hydrated corona (Figure S17e,f).

In order to reduce the strength of electrostatic repulsions between PTMC-Q blocks, we decreased the cationic segment thus reducing the volume of the quaternary ammonium block. In contrast to the behavior of $TerP_{22}$-Q_{20}, the self-assembly of $TerP_{22}$-Q_{11} clearly showed a response to ionic strength during the hydration step. When hydrated in Milli-Q water, $TerP_{22}$-Q_{11} formed uniform spherical micelles (SMs) with hydrodynamic radius (R_h) of ≈22 nm (**Figure 2**a). Cryo-TEM microscopy, AF4-MALS, and DLS confirmed the presence of SMs in samples of $TerP_{22}$-Q_{11} hydrated in Milli-Q water (Figure 2c). Indeed, $TerP_{22}$-Q_{11} SMs eluted after 10–12 min with ρ values ranging from 0.7 to 0.75 (Figure 2e). However, when $TerP_{22}$-Q_{11} was hydrated into salt solution with [NaCl] ≥ 100 × 10^{-3} M, DLS measurements clearly identified a change in nanoparticle morphology with the presence of a significant population at >100 nm (Figure 2a,b; Figure S18, Supporting Information). Cryo-TEM clearly identified this new morphology as nanoworms (NWs) in samples of $TerP_{22}$-Q_{11} hydrated into 100–400 × 10^{-3} M NaCl (Figure 2d; Figure S19, Supporting

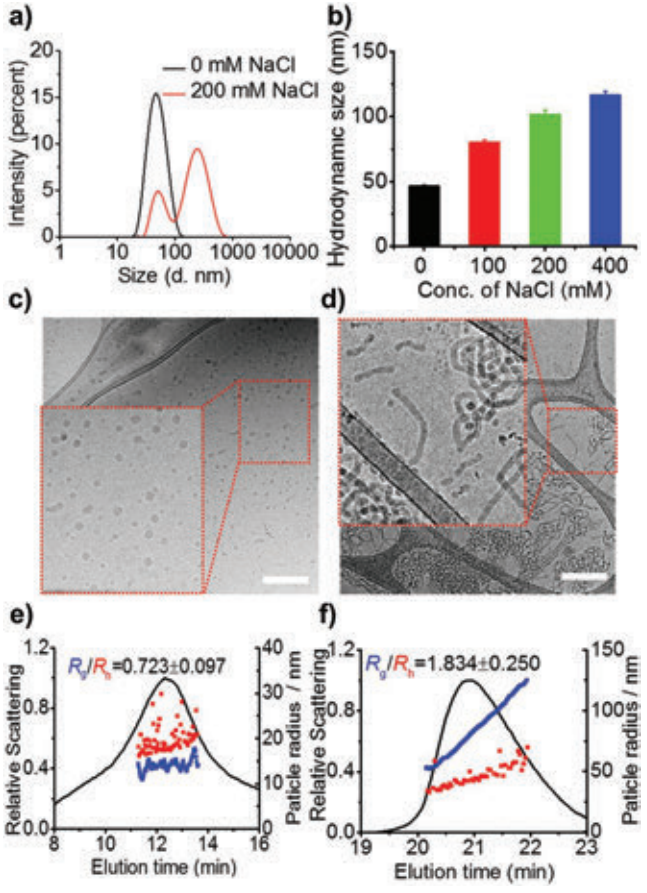

Figure 2. Well-defined spherical micelles (SMs) and elongated nanoworms (NWs) comprising $TerP_{22}$-Q_{11} terpolymers. a) DLS curve of $TerP_{22}$-Q_{11} terpolymers hydrated in Milli-Q or 200 × 10^{-3} M NaCl. b) Hydrodynamic size determined by DLS measurement of $TerP_{22}$-Q_{11} terpolymers hydrated in different concentrations of NaCl. Cryo-TEM images of c) SMs and d) NWs (scale bars = 200 nm). AF4 fractogram (scattering profile in black) of e) SMs hydrated in Milli-Q and f) NWs hydrated in 200 × 10^{-3} M NaCl, comparing the radius of gyration (R_g, blue) to the hydrodynamic radius (R_h, red).

Information). Using AF4, NWs eluted later than SMs (after 20–22 min) and possessed characteristic shape factor (ρ) values of ≈1.8–2.3, indicative of highly elongated nanostructures (Figure 2f; Figure S20 and Table S3, Supporting Information). It was apparent from AF4 data that the R_g of NWs tended to increase with [NaCl], which was supported by cryo-TEM images, indicating that increasing ionic strength yielded more elongated worms (Figures S19 and S20, Supporting Information).

To further increase our understanding of this system, gaining further insight into the self-assembly behavior, $TerP_{22}$-Q copolymers with shorter Q block were prepared in order to explore its effect on nanoparticle morphology. Further decreasing the length of the cationic block ($TerP_{22}$-Q_6) seemed to negate the ionically induced morphology switch, as NWs were observed under all conditions. DLS measurements identified that larger (>100 nm) particles formed after hydration of $TerP_{22}$-Q_6 into the water, which persisted at all salt concentrations (Figure S22, Supporting Information). Cryo-TEM clearly identified NWs in the absence and presence of different NaCl concentration solutions (Figure S23, Supporting Information), characterized by ρ values higher than 1.7, which are indicative of highly elongated nanostructures (Figure S24 and Table S4, Supporting Information).

The unique capacity of $TerP_{22}$-Q_n (where n = 6 or 11) to undergo programmed assembly into NWs was evident when contrasted to control polymers like $TerP_{22}$-Br_6 (the synthetic precursor to $TerP_{22}$-Q_6) and $TerP_{22}$-G_5 (where the quaternary ammonium was replaced with a cationic guanidinium moiety—all chemical structures of copolymers synthesized are listed in **Figure 3** and the Supporting Information). Neither $TerP_{22}$-Br_6 nor $TerP_{22}$-G_5 showed any capacity to undergo assembly into well-defined NWs and, instead, formed well-defined SMs (Figure S26, Supporting Information). Although this property was expected from uncharged $TerP_{22}$-Br_6, it was surprising that the cationic guanidinium analogue did not form NWs in the same fashion as the quaternary ammonium derivate $TerP_{22}$-Q_6. This was likely caused by the distinct nature of the head group, $TerP_{22}$-G_5; resulting in higher surface curvature, which could not be overcome even upon addition of up to 400×10^{-3} M NaCl. Presumably, this behavior was caused by the frustrated packing of the side chain and strong hydration forces of the guanidinium moiety, driving the formation of high surface curvature (spherical) micelles.[22] The significant impact molecular design has upon the resulting morphology was furthermore illustrated when the 1 kDa PEG block was replaced by a 2 kDa chain. Indeed, the 2 kDa PEG-based $TerP_{44}$-Q_{20} underwent assembly into elongated NWs at a high concentration of NaCl (Figures S27 and S28, Supporting Information), however, they were significantly reduced in length and the proportion of SMs when hydrated in ≤400×10^{-3} M NaCl solution was much greater compared to the 1 kDa analogue (Figure S27, Supporting Information). The above observations provide evidence to support the role of PTMC-Q in directing the ionically induced morphology switch of $TerP_{22}$ copolymers (Figure 3). Taken together this highlights the unique capacity of $TerP_{22}$-Q BCPs to undergo self-assembly into NWs, programmed into the molecular structure and giving rise to unique supramolecular behavior.

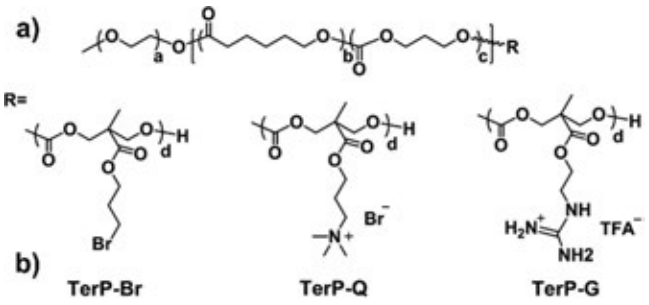

Ter-BCPs	R_g/R_h[i]	Morphology[i]	R_g/R_h[ii]	Morphology[ii]
$TerP_{22}$-Q_6	1.85±0.23	NWs	1.74±0.23	NWs
$TerP_{22}$-Q_{11}	0.72±0.09	SMs	1.82±0.25	NWs
$TerP_{22}$-Q_{20}	0.74±0.16	SMs	0.70±0.26	SMs
$TerP_{44}$-Q_{20}	0.80±0.17	SMs	2.78±0.13	NWs[iii]
$TerP_{22}$-G_5	–	SMs	–	SMs
$TerP_{22}$-Br_6	–	SMs	–	SMs

Figure 3. a) Chemical structure of different terpolymers based on PEG-PCLgPTMC; b) Particle characterization of terpolymers self-assembled via direct hydration into i) water, ii) 200×10^{-3} M, or iii) 600×10^{-3} M NaCl.

2.3. Nanoworms Enhance Cell Membrane Interactions

As already mentioned, high aspect-ratio nanostructures are exciting targets for nanomedical investigation due to their improved biological performance and ability to enhance interactions with living cells.[23] In particular, the ability to direct nanoparticles toward cancer cells, which typically possess more negative surface charge, using electrostatic targeting is an application deserving further investigation as a general strategy to increase the specificity of anticancer therapies.[17a,24] With this in mind, we undertook preliminary testing to explore the advantageous properties of NWs comprising $TerP_{22}$-Q_{11}, comparing them to SMs and an uncharged nanoparticle control system (UPs), comprising PEG_{22}-$PCL_{30}gTMC_{30}$.[11] First, the stability of SMs and NWs comprising $TerP_{22}$-Q_{11} when transferred into PBS or cell culture medium, of critical importance for potential application in biomedical research, was confirmed using DLS (Figures S30–S32, Supporting Information). Particle stability was confirmed when no changes in the correlation data were observed during incubation under physiological conditions. Indeed, sodium dodecyl sulfate (SDS) micelles only undergo spontaneous morphological transitions when [NaCl] reached 1M, which is well above physiological conditions.[25] The critical aggregation concentration (CAC) was determined using a 1-anilino-8-naphthalenesulfonate (ANS) assay. CAC values of SMs were measured at ≈0.030 mg mL^{-1} (2.7×10^{-6} M), with NWs displaying a slightly lower CAC at ≈0.022 mg mL^{-1} (2.0×10^{-6} M) (Figure S33, Supporting Information). Zeta-potential measurements of $TerP_{22}$-Q_{11} SMs and NWs highlighted the same charge characteristics in both systems (as expected) with values of 25 ± 3 mv and 27 ± 4 mV, respectively, which can drive electrostatic interactions with the anionic cancer cell membrane (Figure S34, Supporting Information).

Conducting in vitro studies we found that, indeed, adhesion to cancer cells (HepG2) was enhanced for cationic particles.

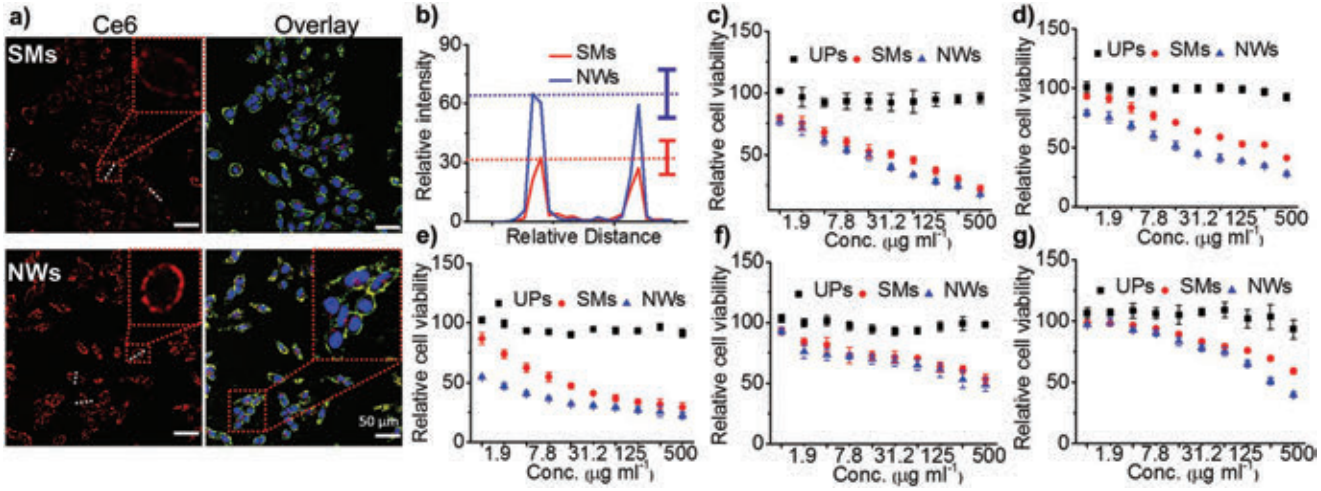

Figure 4. In vitro performance of SMs and NWs comprising $TerP_{22}$-Q_{11}. a) Confocal images of HepG2 cells treated with Ce6-labeled SMs and NWs from $TerP_{22}$-Q_{11} for 2 h (scale bar = 50 μm, blue: Hoechst; green: cell mask; red: NWs.). b) relative fluorescent intensity of red channels in a) analyzed by Image J. Cell viability of c) HeLa cells, d) HepG2 cells, e) MCF-7 cells, f) MCF-7/ADR, and g) NIH 3T3 cells after treatment with different concentrations of PEG-PCLgTMC nanoparticles (UPs), SMs, and NWs.

Elongated NWs showed a twofold increase in binding to cancer cell membranes as compared to SMs, which is understandable given the polyvalent nature of interactions between high aspect ratio structures and the external cell membrane (**Figures 4**a,b and Figure S35 of the Supporting Information). To explore the potential of cationic NWs to interact specifically with cancer cells we compared the effect of the presence of NWs on the viability of HeLa, HepG2, and MCF-7 cells with multidrug resistant MCF-7/ADR and healthy fibroblast (NIH 3T3) cells (Figure 4c–g). Uncharged control particles (UPs) did not show any significant toxicity toward any cell lines at concentrations of up to 0.5 mg mL^{-1} (cell viability ≥ 90%). However, both SMs and NWs displayed toxicity toward cancer cells, as evidenced by the low IC_{50} in HeLa cells (SMs IC_{50}: 28.41 μg mL^{-1}. NWs IC_{50}: 13.8 μg mL^{-1}; Figure 4c), HepG2 cells (SMs IC_{50}: 207.1 μg mL^{-1}. NWs IC_{50}: 27.9 μg mL^{-1}; Figure 4d), and MCF-7 cells (SMs IC_{50}: 21.0 μg mL^{-1}. NWs IC_{50}: 1.1 μg mL^{-1}; Figure 4e, Table S6 of the Supporting Information). This toxicity was significantly reduced with drug-resistant cell line MCF-7/ADR (SMs IC_{50} > 500 μg mL^{-1}; NWs IC_{50}: 419 μg mL^{-1}; Figure 4f), or healthy cell line NIH 3T3 (SMs IC_{50} > 500 μg mL^{-1}; NWs IC_{50}: 354 μg mL^{-1}; Figure 4g). Specific toxicity against cancer cells can be explained by the higher abundance of anionic lipids in the lipid membrane; this selectivity of the cationic polymer assemblies for cancer cells highlights their therapeutic potential. However, we should note that this specificity does not necessarily extend to all cancer cell types, with drug-resistant MCF-7/ADR cells resisting this behavior.

2.4. Penetration into 3D Tumor Multicellular Spheroids

Furthermore, to demonstrate the capacity of NWs toward anticancer therapy we examined their ability to penetrate into a 3D tumor model. Indeed, we found that the enhanced interactions between NWs and the cell membrane, besides the distinctive elongated morphology, resulted in improved permeation into 3D multicellular spheroids comprising cancer and healthy fibroblast cells (HeLa:3T3 = 1:5) (**Figure 5**a).[26] After 18 h incubation, it was apparent that BODIPY-labeled NWs outperformed Chlorin e6 (Ce6)-labeled SMs in the same spheroid—a property uniquely connected to their morphology due to the identical nature of the BCPs in both cases (Figure S36, Supporting Information). Furthermore, incubation of spheroids with either BODIPY-labeled SMs or BODIPY-labeled NWs further confirmed this, highlighting that high-aspect ratio NWs have enhanced tumor penetration propensity under physiological conditions (Figure S37, Supporting Information). Although this enhanced penetration can potentially be tuned through closer control over the aspect ratio of asymmetric nanoparticles,[27] our present system possesses a relatively wide range of aspect ratios in excess of 4 (according to cryo-TEM data, cf. Figure S19 of the Supporting Information).

2.5. Chemotherapy toward MDR Cells

Loading particles with a model chemotherapeutic drug (doxorubicin, DOX) was conducted in order to demonstrate drug delivery capacity that, when combined with electrostatic targeting of cancer cells, could have potential as a nanomedical technology.[28] DOX-loaded SMs and NWs (fabricated with 83 ± 6% efficiency and 4.1 ± 0.3 wt% loading; Figure S38, Supporting Information) showed effective delivery into cells after only 1 h incubation time, concomitant with particle uptake by cells (Figure 5b; Figure S39, Supporting Information). Significantly, SMs and NWs were able to improve the DOX retention in the cell nucleus against a resistant cell line (MCF-7/ADR), when compared with free DOX and DOX-loaded UPs (**Figure 6**a; Figures S40 and S41, Supporting Information). This effect was likely enhanced through strong interactions with (and subsequent destabilization of) the plasma membrane. Indeed, increased permeability of MCF-7/ADR cells (as indicated by propidium iodide, PI, signal—Figure 6b; Figure S42,

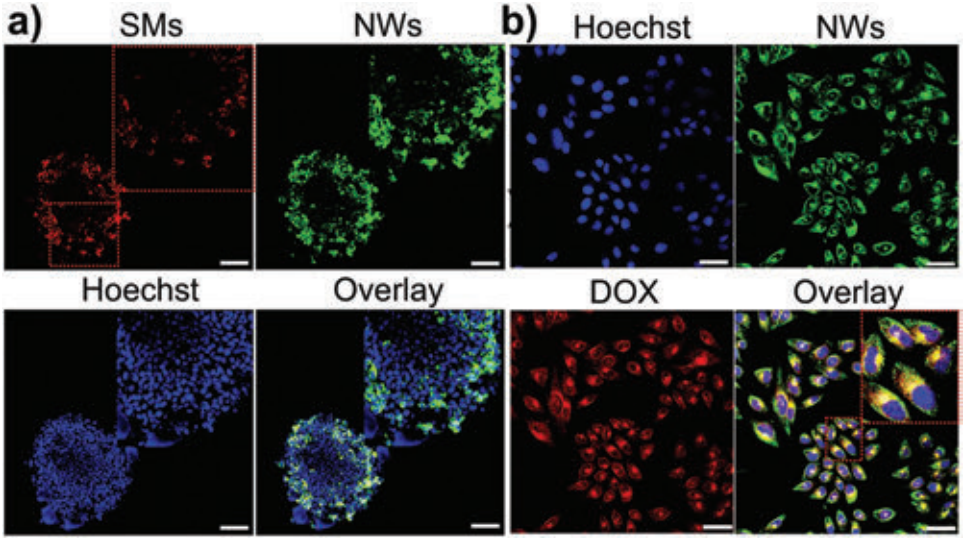

Figure 5. In vitro performance of SMs and NWs comprising $TerP_{22}$-Q_{11}. a) Confocal images displaying penetration of SMs and NWs coincubated with 3D HeLa: 3T3 multicellular spheroids (MCSs, Scanning depth: 30 µm. Blue: Hoechst; Green: BODIPY dye-labeled NWs; Red: SMs, scale bar = 100 µm, inset: zoom in of the imaging). b) Confocal images of HepG2 cells treated with DOX-loaded NWs for 1 h (scale bar = 50 µm. Blue: Hoechst; Green: BODIPY dye-labeled NWs; Red: DOX).

Supporting Information) and enhanced ROS induction (Figure 6c; Figure S43, Supporting Information) after incubation with SMs and NWs (as compared to UPs) clearly demonstrated the destabilizing effect of these charged nanoparticles. As a result, SMs and NWs were able to improve the efficacy of DOX against MCF-7/ADR cells, decreasing the IC_{50} from > 25 µg mL^{-1} down to 3.0 and 1.9 µg mL^{-1}, respectively (Figure 6d; Table S7, Supporting Information), as compared to UPs. Even though specific binding to MCF-7/ADR cells was not as pronounced as other cancer cell lines, a marked increase in the efficacy of DOX was observed, likely due to enhanced drug bioavailability within this resistant cell line. Such mechanisms for overcoming drug-resistance, by enhancing intracellular drug delivery, can provide exciting new pathways for anticancer therapeutics.[29]

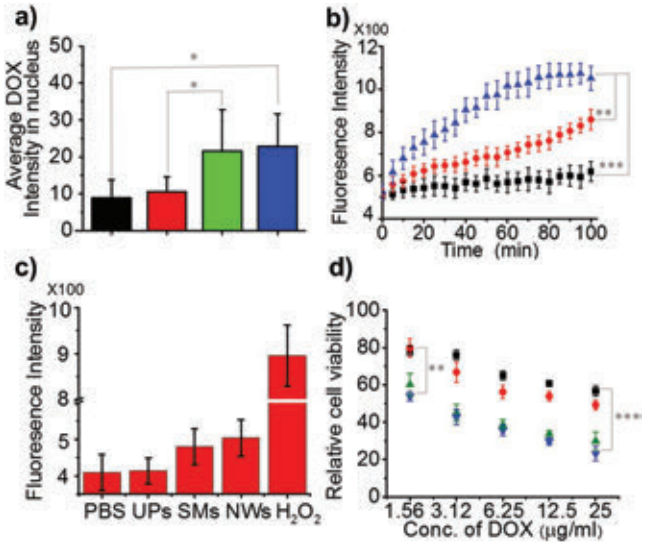

Figure 6. In vitro performance of drug-loaded SMs and NWs comprising $TerP_{22}$-Q_{11}. a) Average DOX intensity in the nucleus obtained by confocal images and analyzed by Image J after cells were incubated with free DOX (black), DOX@UPs (red), DOX@SMs (green) or DOX@NWs (blue). b) Fluorescence intensity of propidium iodide (PI) in MCF-7/ADR cells and c) intracellular ROS (assessed by CM-DCF fluorescence) after treatment with PBS, 500 µg mL^{-1} of UPs (black), SMs (red), or NWs (blue) (for 24 h and using 0.5×10^{-3} M H_2O_2 challenge for 5 min as a control in the ROS study). d) Cell viability of MCF-7/ADR cells after treatment with either free DOX (black), DOX@UPs (red), DOX@SMs (green), or DOX@NWs (blue). Significance was assessed using one-way ANOVA, followed by Tukey's multiple comparisons test (*$P < 0.05$, **$P < 0.01$, ***$P < 0.001$).

3. Conclusion

In summary, we have applied the direct hydration approach for the preparation of well-controlled biodegradable nanoworms, with high-aspect ratio, generated through an ionically induced morphology switch of cationic terpolymer molecules. This provides a new direction for the engineering of nanoparticles with tailored morphologies and properties that can be applied as therapeutic carriers for synergistic drug delivery. Although the biochemical mechanism will certainly need further exploration, the observed cancer specificity of positively charged nanoworms (with improved tumor penetration and directed drug uptake) makes this an exciting system, with great potential for biomedical research where shape and size control is of critical importance.

Supporting Information

Supporting Information is available from the Wiley Online Library or from the author.

Acknowledgements

The authors would like to acknowledge the ERC Advanced Grant Artisym 694120, the Dutch Ministry of Education, Culture and Science (Gravitation program 024.001.035), the NWO-NSFC Advanced Materials (project 792.001.015), and the European Union's Horizon 2020 research and innovation programme Marie Sklodowska-Curie Innovative Training Networks Nanomed (No. 676137) for funding. We thank the Ser Cymru II programme for support of DSW; this project received funding from the European Union's Horizon 2020 research and innovation programme under the Marie Skłodowska-Curie grant agreement No. 663830. This work was also supported by research funding from the National Natural Science Foundation of China (NSFC 51561135010). We also thank Imke Pijpers and Alex Mason for help with Cryo-TEM measurements.

Conflict of Interest

The authors declare no conflict of interest.

Keywords

drug delivery, nanomedicine, nanostructures, self-assembly

Received: April 11, 2019
Revised: July 11, 2019
Published online: August 5, 2019

[1] a) Y. Geng, P. Dalhaimer, S. Cai, R. Tsai, M. Tewari, T. Minko, D. E. Discher, *Nat. Nanotechnol.* **2007**, *2*, 249; b) J. J. Green, J. H. Elisseeff, *Nature* **2016**, *540*, 386; c) S. Mitragotri, J. Lahann, *Nat. Mater.* **2009**, *8*, 15; d) S. Venkataraman, J. L. Hedrick, Z. Y. Ong, C. Yang, P. L. R. Ee, P. T. Hammond, Y. Yang, *Adv. Drug Delivery Rev.* **2011**, *63*, 1228.

[2] a) X. Hu, J. Hu, J. Tian, Z. Ge, G. Zhang, K. Luo, S. Liu, *J. Am. Chem. Soc.* **2013**, *135*, 17617; b) M. Mullner, S. J. Dodds, T. H. Nguyen, D. Senyschyn, C. J. H. Porter, B. J. Boyd, F. Caruso, *ACS Nano* **2015**, *9*, 1294; c) Y. Chang, Y. Lv, P. Wei, P. Zhang, L. Pu, X. Chen, K. Yang, X. Li, Y. Lu, C. Hou, Y. Pei, W. Zeng, Z. Pei, *Adv. Funct. Mater.* **2017**, *27*, 1703083.

[3] a) R. Agarwal, V. Singh, P. Jurney, L. Shi, S. V. Sreenivasan, K. Roy, *Proc. Natl. Acad. Sci. U S A* **2013**, *110*, 17247; b) D. Li, Z. Tang, Y. Gao, H. Sun, S. Zhou, *Adv. Funct. Mater.* **2016**, *26*, 66; c) C. Kinnear, T. L. Moore, L. Rodriguez-Lorenzo, B. Rothen-Rutishauser, A. Petri-Fink, *Chem. Rev.* **2017**, *117*, 11476; d) Q. Sun, T. Ojha, F. Kiessling, T. Lammers, Y. Shi, *Biomacromolecules* **2017**, *18*, 1449.

[4] a) D. S. Williams, I. A. B. Pijpers, R. Ridolfo, J. C. M. van Hest, *J. Controlled Release* **2017**, *259*, 29; b) Y. Hou, S. Cao, L. Wang, Y. Pei, G. Zhang, S. Zhang, Z. Pei, *Polym. Chem.* **2015**, *6*, 223.

[5] a) J. Shao, M. Abdelghani, G. Shen, S. Cao, D. S. Williams, J. C. M. van Hest, *ACS Nano* **2018**, *12*, 4877; b) M. Xuan, Z. Wu, J. Shao, L. Dai, T. Si, Q. He, *J. Am. Chem. Soc.* **2016**, *138*, 6492.

[6] Z. Li, J. Ma, N. S. Lee, K. L. Wooley, *J. Am. Chem. Soc.* **2011**, *133*, 1228.

[7] a) J. R. Lovett, N. J. Warren, L. P. D. Ratcliffe, M. K. Kocik, S. P. Armes, *Angew. Chem., Int. Ed.* **2015**, *54*, 1279; b) M. J. Derry, O. O. Mykhaylyk, S. P. Armes, *Angew. Chem., Int. Ed.* **2017**, *56*, 1746.

[8] a) F. H. Schacher, P. A. Rupar, I. Manners, *Angew. Chem., Int. Ed.* **2012**, *51*, 7898; b) X. Li, Y. Gao, R. Harniman, M. Winnik, I. Manners, *J. Am. Chem. Soc.* **2016**, *138*, 12902; c) J. R. Finnegan, X. He, S. T. G. Street, J. D. Garcia-Hernandez, D. W. Hayward, R. L. Harniman, R. M. Richardson, G. R. Whittell, I. Manners, *J. Am. Chem. Soc.* **2018**, *140*, 17127.

[9] a) L. K. E. A. Abdelmohsen, D. S. Williams, J. Pille, S. G. Ozel, R. S. M. Rikken, D. A. Wilson, J. C. M. van Hest, *J. Am. Chem. Soc.* **2016**, *138*, 9353; b) I. A. B. Pijpers, L. K. E. A. Abdelmohsen, D. S. Williams, J. C. M. van Hest, *ACS Macro Lett.* **2017**, *6*, 1217.

[10] W. Li, T. Suzuki, H. Minami, *Angew. Chem., Int. Ed.* **2018**, *57*, 9936.

[11] L. M. P. E. van Oppen, L. K. E. A. Abdelmohsen, S. E. van Emst-de Vries, P. L. W. Welzen, D. A. Wilson, J. A. M. Smeitink, W. J. H. Koopman, R. Brock, P. H. G. M. Willems, D. S. Williams, J. C. M. van Hest, *ACS Cent. Sci.* **2018**, *4*, 917.

[12] a) R. Ridolfo, B. C. Ede, P. Diamanti, P. B. White, A. W. Perriman, J. C. M. van Hest, A. Blair, D. S. Williams, *Small* **2018**, *14*, 1703774; b) S. Cao, L. K. E. A. Abdelmohsen, J. Shao, J. van den Dikkenberg, E. Mastrobattista, D. S. Williams, J. C. M. van Hest, *ACS Macro Lett.* **2018**, *7*, 1394.

[13] a) K. Han, J. Zhang, W. Zhang, S. Wang, L. Wu, C. Zhang, X. Zhang, H. Han, *ACS Nano* **2017**, *11*, 3178; b) C. Lu, M. W. Urban, *Prog. Polym. Sci.* **2018**, *78*, 24; c) S. H. Kim, F. Nederberg, R. Jakobs, J. P. K. Tan, K. Fukushima, A. Nelson, E. W. Meijer, Y. Yang, J. L. Hedrick, *Angew. Chem., Int. Ed.* **2009**, *48*, 4508; d) Q. Yan, Y. Zhao, *Angew. Chem., Int. Ed.* **2013**, *52*, 9948; e) T. Sun, Y. Zhang, B. Pang, D. Hyun, M. Yang, Y. Xia, *Angew. Chem. Int. Ed.* **2014**, *53*, 12320; f) M. Elsabahy, K. L. Wooley, *Chem. Soc. Rev.* **2012**, *41*, 2545; g) L. A. Fielding, J. A. Lane, M. J. Derry, O. O. Mykhaylyk, S. P. Armes, *J. Am. Chem. Soc.* **2014**, *136*, 5790; h) C. Chen, R. A. L. Wylie, D. Klinger, L. A. Connal, *Chem. Mater.* **2017**, *29*, 1918; i) H. Che, S. Cao, J. C. M. van Hest, *J. Am. Chem. Soc.* **2018**, *140*, 5356.

[14] A. Hanisch, A. H. Groschel, M. Fortsch, M. Drechsler, H. Jinnai, T. M. Ruhland, F. H. Schacher, A. H. E. Muller, *ACS Nano* **2013**, *7*, 4030.

[15] J. Shao, I. A. B. Pijpers, S. Cao, D. S. Williams, X. Yan, J. Li, L. K. E. A. Abdelmohsen, J. C. M. van Hest, *Adv. Sci.* **2019**, *6*, 1801678.

[16] a) K. Fukushima, J. P. K. Tan, P. A. Korevaar, Y. Y. Yang, J. Pitera, A. Nelson, H. Maune, D. J. Coady, J. E. Frommer, A. C. Engler, Y. Huang, K. Xu, Z. Ji, Y. Qiao, W. Fan, L. Li, N. Wiradharma, E. W. Meijer, J. L. Hedrick, *ACS Nano* **2012**, *6*, 9191; b) K. Fukushima, S. Liu, H. Wu, A. C. Engler, D. J. Coady, H. Maune, J. Pitera, A. Nelson, N. Wiradharma, S. Venkataraman, Y. Huang, W. Fan, J. Ying, Y. Yang, J. L. Hedrick, *Nat. Commun.* **2013**, *4*, 2861; c) V. V. Shuvaev, M. A. Ilies, E. Simone, S. Zaitsev, Y. Kim, S. Cai, A. Mahmud, T. Dziubla, S. Muro, D. E. Discher, V. R. Muzykantov, *ACS Nano* **2011**, *5*, 6991.

[17] a) B. Chen, W. Le, Y. Wang, Z. Li, D. Wang, L. Ren, L. Lin, S. Cui, J. Hu, Y. Hu, P. Yang, R. C. Ewing, D. Shi, Z. Cui, *Theranostics* **2016**, *6*, 1887; b) S. K. Samal, M. Dash, S. Van Vlierberghe, D. L. Kaplan, E. Chiellini, C. van Blitterswijk, L. Moroni, P. Dubruel, *Chem. Soc. Rev.* **2012**, *41*, 7147.

[18] a) W. S. Shim, J. H. Kim, H. Park, K. Kim, I. C. Kwon, D. S. Lee, *Biomaterials* **2006**, *27*, 5178; b) N. Kamaly, B. Yameen, J. Wu, O. C. Farokhzad, *Chem. Rev.* **2016**, *116*, 2602.

[19] A. F. Mason, B. C. Buddingh, D. S. Williams, J. C. M. van Hest, *J. Am. Chem. Soc.* **2017**, *139*, 17309.

[20] S. Liu, C. Yang, Y. Huang, X. Ding, Y. Li, W. Fan, J. L. Hedrick, Y. Yang, *Adv. Mater.* **2012**, *24*, 6484.

[21] a) A. Blanazs, S. P. Armes, A. J. Ryan, *Macromol. Rapid Commun.* **2009**, *30*, 267; b) W. Bai, C. A. Ross, *MRS Bull.* **2016**, *41*, 100; c) J. Qian, M. Zhang, I. Manners, M. A. Winnik, *Trends Biotechnol.* **2010**, *28*, 84.

[22] a) J. Werner, E. Wernersson, V. Ekholm, N. Ottosson, G. Ohrwall, J. Heyda, I. Persson, J. Soderstrom, P. Jungwirth, O. Bjorneholm, *J. Phys. Chem. B* **2014**, *118*, 7119; b) R. Mogaki, P. K. Hashim, K. Okuro, T. Aida, *Chem. Soc. Rev.* **2017**, *46*, 6480.
[23] a) P. Kolhar, A. C. Anselmo, V. Gupta, K. Pant, B. Prabhakarpandian, E. Ruoslahti, S. Mitragotri, *Proc. Natl. Acad. Sci. U S A* **2013**, *110*, 10753; b) S. Barua, J. W. Yoo, P. Kolhar, A. Wakankar, Y. R. Gokarn, S. Mitragotri, *Proc. Natl. Acad. Sci. U S A* **2013**, *110*, 3270.
[24] J. Zhao, S. M. Wu, J. W. Qin, D. L. Shi, Y. L. Wang, *ACS Appl. Mater. Interfaces* **2018**, *10*, 41986.
[25] G. V. Jensen, R. Lund, J. Gummel, T. Narayanan, J. S. Pedersen, *Angew. Chem., Int. Ed.* **2014**, *53*, 11524.
[26] a) V. P. Chauhan, Z. Popovic, O. Chen, J. Cui, D. Fukumura, M. G. Bawendi, R. K. Jain, *Angew. Chem., Int. Ed.* **2011**, *50*, 11417; b) B. R. Smith, P. Kempen, D. Bouley, A. Xu, Z. Liu, N. Melosh, H. J. Dai, R. Sinclair, S. S. Gambhir, *Nano Lett.* **2012**, *12*, 3369.
[27] a) S. Shukla, F. J. Eber, A. S. Nagarajan, N. A. DiFranco, N. Schmidt, A. M. Wen, S. Eiben, R. M. Twyman, C. Wege, N. F. Steinmetz, *Adv. Healthcare Mater.* **2015**, *4*, 874; b) M. Mullner, K. Yang, A. Kaur, E. J. New, *Polym. Chem.* **2018**, *9*, 3461; c) J. Wang, W. Mao, L. L. Lock, J. Tang, M. Sui, W. Sun, H. Cui, D. Xu, Y. Shen, *ACS Nano* **2015**, *9*, 7195.
[28] a) S. Cao, Z. Pei, Y. Xu, Y. Pei, *Chem. Mater.* **2016**, *28*, 4501; b) K. Yang, Y. Chang, J. Wen, Y. Lu, Y. Pei, S. Cao, F. Wang, Z. Pei, *Chem. Mater.* **2016**, *28*, 1990; c) Y. Chang, C. Hou, J. Ren, X. Xin, Y. Pei, Y. Lu, S. Cao, Z. Pei, *Chem. Commun.* **2016**, *52*, 9578.
[29] C. Peetla, R. Bhave, S. Vijayaraghavalu, A. Stine, E. Kooijman, V. Labhasetwar, *Mol. Pharmaceutics* **2010**, *7*, 2334.